Permeant Cations and Blockers Modulate pH Gating of ROMK Channels

H. Sackin, A. Vasilyev, L. G. Palmer,* and M. Krambis
Department of Physiology and Biophysics, The Chicago Medical School, North Chicago, Illinois 60064; and
*Department of Physiology and Biophysics, Weill Medical College of Cornell University, New York, New York 10021

ABSTRACT External potassium (K) activates the inward rectifier ROMK ($K_{ir}1.1$) by altering the pH gating of the channel. The present study examines this link between external K and internal pH sensitivity using both the two-electrode voltage clamp and the perfused, cut-open *Xenopus* oocyte preparation. Elevating extracellular K from 1 mM to 10 mM to 100 mM activated ROMK channels by shifting their apparent pK_a from 7.2 ± 0.1 ($n = 6$) in 1 mM K, to 6.9 ± 0.02 ($n = 5$) in 10 mM K, and to 6.6 ± 0.03 ($n = 5$) in 100 mM K. At any given internal pH, the number of active ROMK channels is a saturating function of external [K]. Extracellular Cs (which blocks almost all inward K current) also stimulated outward ROMK conductance (at constant 1 mM external K) by shifting the apparent pK_a of ROMK from 7.2 ± 0.1 ($n = 6$) in 1 mM K to 6.8 ± 0.01 ($n = 4$) in 1 mM K + 104 mM Cs. Surprisingly, the binding and washout of the specific blocker, Tertiapin-Q, also activated ROMK in 1 mM K and caused a comparable shift in apparent pK_a. These results are interpreted in terms of both a three-state kinetic model and a two-gate structural model that is based on results with KcsA in which the selectivity filter can assume either a high or low K conformation. In this context, external K, Cs, and Tertiapin-Q activate ROMK by destabilizing the low-K (collapsed) configuration of the selectivity filter.

INTRODUCTION

Potassium (K) secretion into the lumen of the renal CCT and TAL is largely mediated by ROMK inward rectifier channels (Palmer et al., 1997) that are regulated by intracellular pH in both native tubules (Wang and Giebisch, 1991; Wang et al., 1992) and oocyte expression systems (McNicholas et al., 1998; Doi et al., 1996; Fakler et al., 1996; Tsai et al., 1995; Choe et al., 1997). The sensitivity of the ROMK family to internal (but not external) pH depends on a single lysine residue: K61 in ROMK2 (K80 in ROMK1; Fakler et al., 1996), although other nearby residues also influence pH gating (Choe et al., 1997). The homologous IRK1 channel (K_{ir} 2.1) has a *Met* at this position and is insensitive to intracellular pH above 6.5 (Fakler et al., 1996; Choe et al., 1997).

The strong sensitivity of ROMK to internal pH is modulated by phosphorylation of three serine residues on the intracellular side of the channel (McNicholas et al., 1994; Leipziger et al., 2000). In addition, ROMK activity is also modulated by extracellular K, where low external K (corresponding to low luminal K in the nephron) decreases the number of active ROMK channels and high external K (between 10 mM and 100 mM) increases the number of active ROMK channels (Sackin et al., 2001; Schulte et al., 2001; Doi et al., 1996).

The mechanism responsible for this effect of external K on ROMK activity depends on specific residues at both the extracellular side of ROMK2 (F129, Q133, and E132) and within the pore (V121 and L117; Sackin et al., 2001; Schulte et al., 2001). Replacing any of these residues by their IRK1 homologs renders ROMK insensitive to the effects of external K removal. In the present study, we further explore this mechanism using the honeybee toxin, Tertiapin-Q (TPNQ) which not only blocks conduction through ROMK (Jin and Lu, 1998; Jin et al., 1999), but also appears to pull ROMK channels out of their inactivated state. This ''stimulatory'' effect of the blocker TPNQ may provide insight into the nature of the coupling between external K and internal pH.

METHODS

Construction of chimeras and point mutants of ROMK

Chimeras were constructed using the splicing by overlap extension method (Horton et al., 1989) as described in Choe et al. (1999), using parts of either ROMK2 (GenBank accession # L29403) or IRK1 (GenBank accession # X73052). The C9 chimera was formed by replacing the PM region of ROMK by the homologous region of IRK (Fig. 1). Point mutations in both ROMK2 and the C9 chimera were engineered with a PCR QuikChange site-directed mutagenesis kit, where primers were synthesized by Integrated DNA Technologies, Inc (Coralville, IA). Nucleotide sequences between two restriction enzyme sites were checked using an ABI Prism 377XL automated DNA sequencer at The University of Chicago Cancer Research Center.

Expression of channels

Plasmids were linearized with *Not*I restriction enzyme and transcribed in vitro with T7 RNA polymerase in the presence of the GpppG cap using mMESSAGE mMACHINE kit (Ambion, Austin, TX). Synthetic cRNA was dissolved in water and stored at −70°C before use. Stage V–VI oocytes were obtained by partial ovariectomy of female *Xenopus laevis* (NASCO, Ft. Atkinson, WI), anesthetized with tricaine methanesulfonate (1.5 g/L,

Submitted April 18, 2002, and accepted for publication August 23, 2002.

Address reprint requests to Dr. Henry Sackin, Dept. of Physiology and Biophysics, The Chicago Medical School, 3333 Green Bay Rd., North Chicago, IL 60064. Tel.: 847-578-8329; Fax: 847-578-3265; E-mail: sackinh@mis.finchcms.edu.

0006-3495/03/02/910/12 $2.00

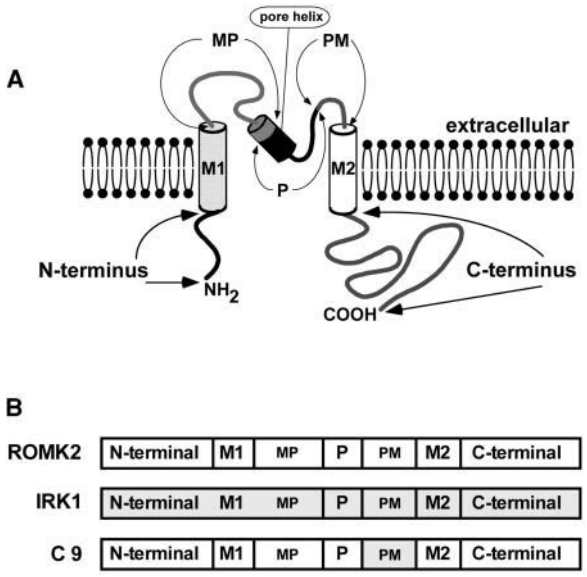

FIGURE 1 The seven segments of ROMK and IRK, and the C9 chimera. (*A*) Both ROMK and IRK consist of four identical subunits surrounding a central pore. Based on hydropathy analysis, we designated seven homologous regions of both the ROMK and IRK subunits: the N-terminus, which is wholly cytoplasmic, the first (or outer) transmembrane segment (*M1*), the MP region which lies between M1 and the pore region, the P or pore region (also referred to as *H5*). The last three residues of MP and the first half of the P region are α-helical. The PM region which lies between the P region and the second (or inner) transmembrane segment (M2), and finally the C-terminus, which is completely cytoplasmic. (*B*) Block diagram showing that in the C9 chimera, the PM region of ROMK has been replaced by the homologous PM region of IRK.

adjusted to pH 7.0). Oocytes were defolliculated by incubation in OR2 solution (82.5 mM NaCl, 2 mM KCl, 1 mM $MgCl_2$, and 5 mM HEPES, adjusted to pH 7.5 with NaOH) containing 2 mg/ml collagenase type II and 2 mg/ml hyaluronidase type II (Sigma Chemical, St. Louis, MO) for 90 min and (if necessary) another 90 min in a fresh enzyme solution at 23°C. Oocytes were injected with 0.5 to 1 ng of cRNA and incubated at 19°C in 2× diluted Leibovitz medium (Life Technologies, Grand Island, NY) for 1 to 4 days before measurements were made.

Whole-cell experiments (two-electrode voltage clamp)

Whole-cell conductances were measured in intact oocytes expressing either ROMK2, a chimera derived from ROMK2 and IRK1, or a mutant of ROMK2 using a two-electrode voltage clamp (TEVC).

Although ROMK is a weak inward rectifier, the whole-cell current voltage relations are approximately linear for small outward currents (Sackin et al., 2001) and outward conductances were determined between an oocyte potential of E_{rest} and E_{rest} + 40 mV using 13 voltage command pulses (25-ms duration, 20-mV increments) centered around the oocyte resting potential. Between each pulse cycle the oocyte was left unclamped in the open-circuit (zero current) condition.

pH titration curves were also obtained in intact oocytes using the TEVC and permeant acetate buffers to control intracellular pH. The relation between intracellular and extracellular pH was calculated from a previous calibration with ROMK oocytes to be $pH_i = 0.595 \times pH_o + 2.4$ (Choe et al., 1997). When impermeant buffers were used, ROMK was essentially insensitive to alterations in external pH.

Cut-open oocyte experiments

The cut-open oocyte preparation was used in those experiments requiring control of intracellular pH to values more alkaline than 7.2. This consisted of a vaseline-gap oocyte chamber fabricated by R.E. Weiss, following the original design of Taglialatela et al. (1992) but modified for internal perfusion of the oocyte, similar to previous reports (Perozo et al., 1992; Costa et al., 1994).

After mounting the oocyte in the multicompartment chamber, but before inserting the voltage microelectrode, a fused silica tubing (100 μm ID, 240 μm OD, #TSP100-245, Polymicro technologies, Phoenix, AZ) was inserted midway through the bottom of the oocyte from below the chamber and perfusion was begun with internal solution at pH 7.8 (or 8.0 for 1 mM K experiments). Internal pH was successively decreased from 7.8 to 7.4, 7.1, 6.8, 6.5, and 6.0 by changing the internal perfusion solution at constant extracellular pH = 7.4. With oocyte perfusion rates of 10 μL/h, 15–20 min were required for equilibration at each new internal pH.

Cut-open oocytes were maintained in the open-circuit condition except for periodic voltage pulses (at 5-min intervals) that were used to generate current-voltage relations at different internal pH values. Outward conductances at successive internal pH values were calculated from the linear portion of the outward current-voltage relation between the reversal potential and 60 mV positive to the reversal potential. Cut-open experiments were performed with ROMK oocytes in external solutions of 1mM K, 10 mM K, 100 mM K, or 104 mM Cs, and with the C9 oocytes in external solutions of 1 mM K or 10 mM K.

Steady state fits to the three-state model

The solver function of Excel was used to minimize the weighted square deviation of the data from the predictions of the model equations. A number of weighting schemes were used, but the most consistent was to weight the deviations by the variance of the average, which gives the greatest weight to the most reliable measurements.

Solutions

Extracellular solutions for intact (TEVC) oocyte experiments

All extracellular solutions for the intact oocyte experiments contained 1mM $MgCl_2$, 2mM $CaCl_2$, 5 mM HEPES and were pH-adjusted to the desired pH with NaOH. Osmolarity was 215 ± 5 mOsmolar, and intracellular pH was controlled with acetate salts, as previously described (Choe et al., 1997). The specific composition for the different cation solutions were:

1. Low K solution: 1 mM KCl, 49 mM NaCl, 55 NaAcetate.
2. 10 mM K solution: 10 mM KCl, 39 mM NaCl, 55 NaAcetate.
3. 97 mM Cs solution: 1 mM KCl, 97 mM CsAcetate. (The rates of oocyte acidification were not appreciably different with 55 mM acetate versus 97 mM acetate.)

Extracellular solutions for cut-open oocyte experiments

The extracellular solutions for the cut-open oocyte experiments all contained 1 mM $MgCl_2$, 2 mM $CaCl_2$, 5 mM HEPES and were pH-adjusted to an extracellular pH of 7.4 with NaOH. Permeant, acetate buffers were not used because intracellular pH was controlled by direct internal perfusion. Osmolarity was 215 ± 5 mOsmolar. The specific composition of the cut-open, external solutions were:

1. Low K solution: 1 mM KCl, 104 mM NaCl.
2. 10 mM K solution: 10 mM KCl, 95 mM NaCl.
3. 100 mM K solution: 100 mM KCl, 5 mM NaCl.
4. 104 mM Cs solution: 1 mM KCl, 104 mM CsCl.

Intracellular solutions for internal perfusion of cut-open oocyte experiments

The internal perfusion solution for the cut-open oocyte experiments consisted of 75 mM KCl, 30 mM NaCl, 5 mM Na_2EDTA, 5 mM HEPES, and was pH-adjusted with NaOH. Osmolarity = 215 ± 5 mOsmolar.

Toxins for intact (TEVC) oocyte experiments

Tertiapin-Q (TPNQ) was obtained from Sigma Aldrich (Cat. # T-1567) as lyophilized powder (0.5 mg). Addition of 1.02 ml of pure water yielded a 200 μM stock solution which was aliquoted into 20 μL volumes and frozen at −20°C in PCR tubes. For each μM of final TPNQ concentration, 5 μL of this stock solution was added to 1 ml of bath solution.

Mamba toxin (δ-dendrotoxin) was obtained from Alamone Labs, Israel as 70 μg lyophilized toxin per vial (Cat. # D-380). Addition of 1.069 ml of pure water to each vial yielded a 10-μM stock solution which was aliquoted into five 200-μL PCR tubes and frozen at −20°C. For each μM of final δ-dendrotoxin solution, 200 μL of this stock solution was added to 2 ml of bath solution.

RESULTS

Fig. 2 illustrates the K-dependence of ROMK pH gating. In these experiments, the outward conductance of intact ROMK oocytes was monitored during decreases and increases of internal pH using permeant acetate buffers to control intracellular pH. Intracellular pH had been previously determined in these buffer solutions, with intracellular pH electrodes and similar ROMK oocytes (Choe et al., 1997).

Internal acidification of the oocytes from pH 7.04 to pH 6.3 (produced by reducing external pH_o from 7.8 to 6.5) abolished outward conductance with a time course that was roughly independent of external K (Fig. 2, *A* vs. *D*). In contrast, the effect of alkalization on outward conductance was strongly dependent on external K. Alkalization with 10 mM external K (Fig. 2 *E*) increased whole-cell conductance much more rapidly, and to a greater extent than the same alkalization in 1 mM external K (Fig. 2 *B*).

Fig. 2 *C* illustrates activation by five different external K concentrations. Starting with most channels inactivated (Fig. 2 *B*, *end*), an abrupt increase in external K increased both the magnitude and rate of channel activation, according to a saturable function (*Inset*, Fig. 2).

Although previous studies (Sackin et al., 2001) have indicated that ROMK single channel conductance increases from 6 pS (in 1 mM external K) to 11 pS (in 10 mM external K), this contribution to whole-cell conductance occurs as soon as K reaches the plasma membrane and is independent of either external or internal pH (Choe et al., 1997). Exchange of the bath solution is complete within 60 seconds. Hence, most of the conductance increase at times greater than $t = 51$ min (Fig. 2 *C*) can be attributed to activation of ROMK channels rather than to changes in single channel conductance. For comparison with subsequent figures, the data of Fig. 2 were normalized to the maximal conductance in 10 mM external K. The inset of Fig. 2 is a plot of nor-

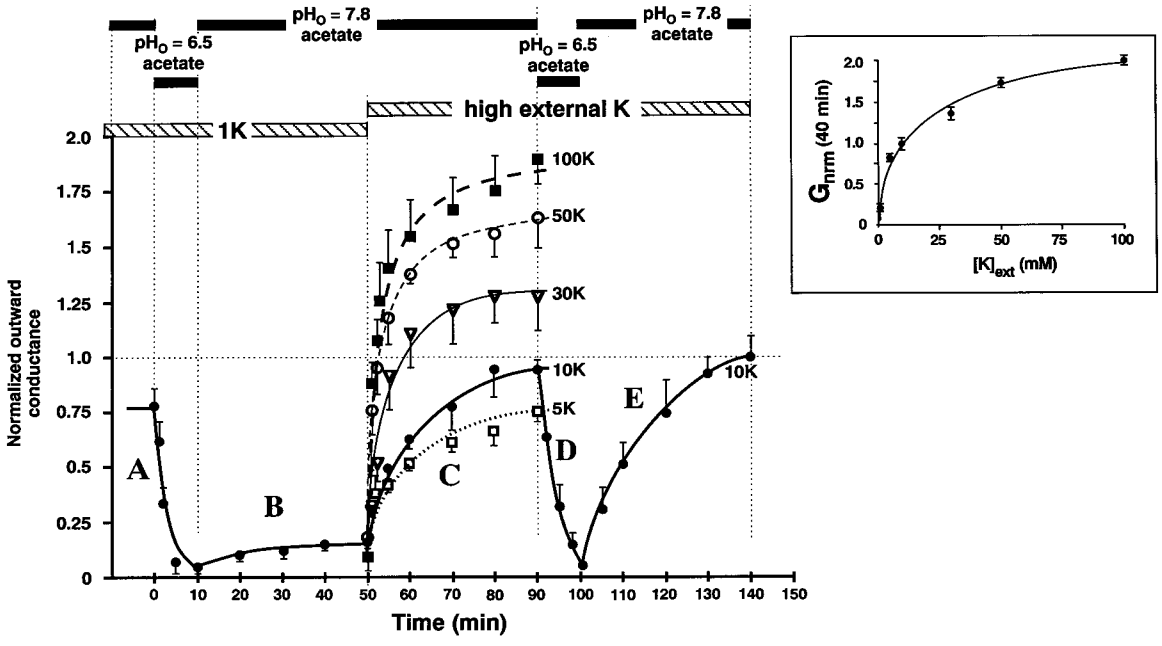

FIGURE 2 Effect of external K on ROMK pH-dependence. Permeant acetate buffers were used to control the internal pH of oocytes expressing ROMK2. Internal pH was calculated using a prior calibration for this buffer system, $pH_i = 0.595 \times \mathrm{pH_o} + 2.4$. Oocytes were first preincubated in 1 mM K at $pH_o = 7.8$ in acetate solutions ($pH_i = 7.04$), and then exposed to a 1 mM K solution at $pH_o = 6.5$ ($\mathrm{pH_i} = 6.3$), followed by a return to $pH_o = 7.8$ acetate solution. After 40 min, external K was raised from 1 mM to 5 mM, 10 mM, 30 mM, 50 mM, or 100 mM external K (still at $pH_o = 7.8$). In the 10 mM external K experiment, extracellular pH_o was reduced for 10 min to 6.5 ($pH_i = 6.3$) and then returned to $pH_o = 7.8$ ($\mathrm{pH_i} = 7.04$). The data are normalized to the maximal conductance in 10 mM external K to facilitate comparison with the other figures. The curves were drawn to fit the data for each condition. The inset is a plot of normalized conductance after 40 min as a function of external $[K]$. A smooth curve is drawn through these points which were not well fit by a single binding site model.

malized conductance after 40 min vs. external [K]. A smooth curve was drawn through these quasi-steady-state conductances, which were not well fit by a single binding site model.

Additional information about the interaction between external K and internal pH is summarized in Fig. 3 which depicts how internal pH modulates activation by external K. In these experiments oocytes were maintained in acetate buffered solutions at either $pH_o = 7.8$ (corresponding to an internal pH of 7.04) or $pH_o = 7.4$ (corresponding to an internal pH of 6.8). With 1 mM external K, decreasing internal pH to 6.3 ($pH_o = 6.5$) inactivated most of the channels, and reduced whole-cell outward conductance close to zero (Fig. 3 *A*). The time course was similar whether oocyte internal pH was held at 7.04 or 6.8 ($pH_o = 7.8$ or $pH_o = 7.4$).

As in Fig. 2, re-alkalization produced only a slight activation of ROMK channels (Fig. 3 *B*) until external K was raised to 10 mM (Fig. 3 *C*). This produced a 5.3 ± 0.9 ($n = 7$)-fold activation of ROMK in the higher pH experiments ($pH_i = 7.04$, $pH_o = 7.8$), and was similar to what had been previously described (Sackin et al., 2001). In the lower pH experiments ($pH_i = 6.8$, $pH_o = 7.4$), raising external K from 1 mM to 10 mM produced a 30 ± 5 ($n = 8$)-fold activation of ROMK conductance, although the time course for the conductance increase was somewhat slower: half time = 8.8 ± 1.1 min at $pH_o = 7.4$ vs. half time = 4.9 ± 1 min at $pH_o = 7.8$.

Upon return of external K, the initial decrease in total conductance was similar at both pH values (Fig. 3, *D* and *E*). At $pH_o = 7.4$ (corresponding to $pH_i = 6.8$) 90% of the activated ROMK channels were inactivated after 50 min. However, at $pH_o = 7.8$ (corresponding to $pH_i = 7.04$), only 25% of the active channels were inactivated after 50 min in 1 mM external K. This represents a strong hysteresis effect. Conditions in Fig. 3, *B* and *D* are identical, but the currents reach different quasi-steady states, depending on whether the channels were initially activated (Fig. 3 *D*) or inactivated (Fig. 3 *B*).

Furthermore, the extent of ROMK inactivation produced by external K removal (Fig. 3, *D* and *E*) depends on the internal pH. In oocytes with lower internal pH (Fig. 3 *E*), K removal inactivates more ROMK channels, producing a lower steady-state total conductance; whereas with oocytes having a higher internal pH (Fig. 3 *D*), K removal produces less inactivation and a higher steady-state conductance. Finally, application of $pH_i = 6.3$ to both groups of ROMK oocytes reduced whole-cell conductance to leak conductance levels (Fig. 3 *F*) and confirmed that the whole-cell conductances were attributable to ROMK.

Cut-open, perfused oocytes were used to control intracellular pH more precisely and to extend the range of intracellular pH to more alkaline values than are possible with intact oocytes. Results of these experiments are shown in Fig. 4 for oocytes expressing ROMK2. Elevation of external K shifted the pH sensitivity of ROMK from an apparent pK_a of 7.2 ± 0.1 ($n = 6$) in 1 mM K, to 6.9 ± 0.02 ($n = 5$) in 10 mM K, and then to 6.6 ± 0.03 ($n = 5$) in 100 mM K. Data were fit to a variable slope, sigmoidal dose-response curve. The fitted Hill coefficients ranged between three and four in a nonsystematic manner, suggesting that either three or four protons per channel were required to

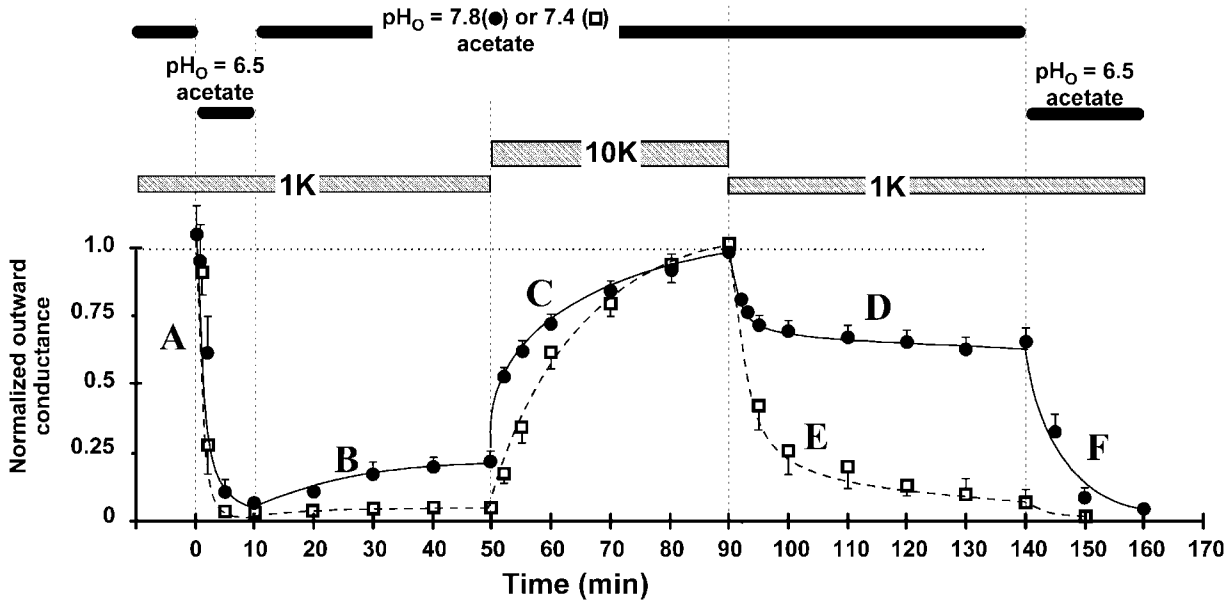

FIGURE 3 Effect of pH on activation and deactivation by external K. Using the same extracellular acetate buffer solutions as in Fig. 2, oocytes expressing ROMK2 were exposed to a 1 mM K solution at $pH_o = 6.5$ ($pH_i = 6.3$), followed by either $pH_o = 7.8$ (*solid line, solid circles*, $pH_i = 7.04$), or $pH_o = 7.4$ (*dashed line, open squares*, $pH_i = 6.8$). After 40 min, external K was raised to 10 mM (still at $pH_o = 7.8$ or 7.4) and maintained at this level for another 40 min. External K was then returned to 1 mM. After 50 min in 1 mM K, pH_o was reduced to 6.5 to confirm that all oocyte conductance was attributable to ROMK. Whole cell outward conductance was determined as in Fig. 2, and data were normalized to the maximum outward conductance in 10 mM K (336 ± 45 μS, $n = 4$ at $pH_o = 7.8$ and 271 ± 22 μS, $n = 6$ at $pH_o = 7.4$).

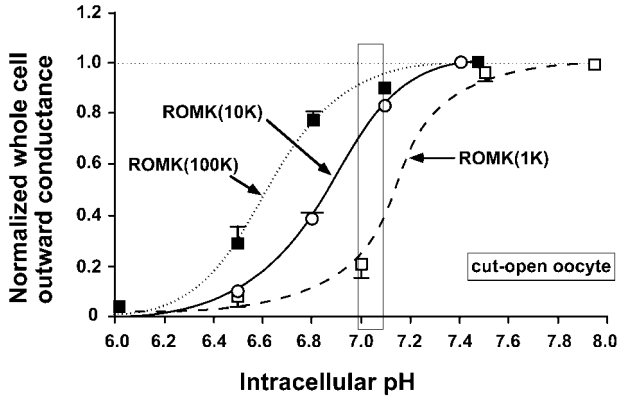

FIGURE 4 K-dependence of the pH gate. The pH gating of ROMK2 was examined at different extracellular [K], using the perfused, cut-open oocyte technique (Methods). (*Open squares, dashed line*) ROMK2 in 1 mM external K (apparent $pK_a = 7.2 \pm 0.1$, $n = 6$). (*Open circles, solid line*) ROMK2 in 10 mM external K (apparent $pK_a = 6.9 \pm 0.02$, $n = 5$). (*Solid squares, dotted line*) ROMK2 in 100 mM external K (apparent $pK_a = 6.6 \pm 0.03$, $n = 5$). Data were fit to a variable slope, sigmoidal dose-response curve. (*Thin rectangle*) Denotes approximate region of normal intracellular pH.

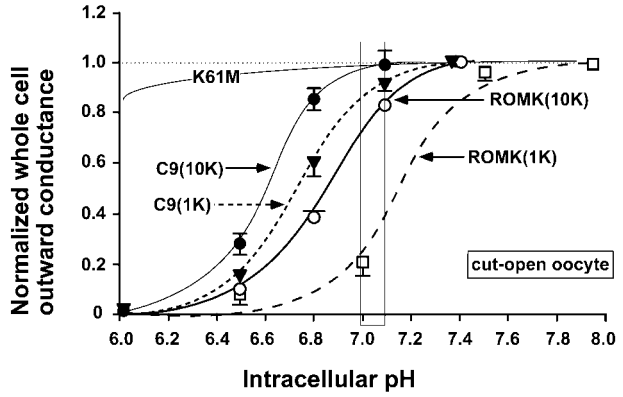

FIGURE 5 K-dependence of the pH gate is structure-dependent. The pH gating of ROMK2 and C9 (a chimera of ROMK2 and IRK1) were compared at different extracellular [K], using the perfused, cut-open oocyte technique (Methods). (*Open squares, dashed line*) ROMK2 in 1 mM external K (apparent $pK_a = 7.2 \pm 0.1$, $n = 6$). (*Open circles, solid line*) ROMK2 in 10 mM external K (apparent $pK_a = 6.9 \pm 0.02$, $n = 5$). (*Solid triangles, dashed line*) C9 in 1 mM external K (apparent $pK_a = 6.7 \pm 0.02$, $n = 4$). (*Solid circles, solid line*) C9 in 10 mM external K (apparent $pK_a = 6.6 \pm 0.02$, $n = 4$). (K61M, *solid line*) Lack of pH-dependence in the ROMK2 mutant, K61M. (*Thin rectangle*) Denotes approximate region of normal intracellular pH. The structure of the C9 chimera, relative to ROMK2, and IRK1 is indicated in Fig. 1.

close the pH gate. This is in reasonable agreement with the estimate of the number of bound protons (α): $3.2 > \alpha > 2.9$, which was derived by fitting the three-state kinetic model to the complete set of data (see Discussion).

The open rectangle illustrates the range of normal internal pH for our oocytes: 7.13 ± .03 (Choe et al., 1997). Raising external K within this range of pH increases whole-cell conductance by activating ROMK channels in a manner consistent with moving from the 1-K curve upward to the 10-K curve in Fig. 4.

In previous studies the C9 chimera (Fig. 1) had a reduced response to changes in extracellular K (Sackin et al., 2001). Given the relationship between K sensitivity and pH sensitivity (Doi et al., 1996; Schulte et al., 2001; Sackin et al., 2001), it makes sense to examine the pH sensitivity of the C9 chimera and compare it to that of ROMK. Fig. 5 indicates that the C9 chimera has a strong sensitivity to intracellular pH but one that is shifted relative to ROMK. Furthermore, an increase in external K from 1 mM to 10 mM decreased the apparent pK_a for C9 by 0.1 pH units (6.7 ± 0.02 to 6.6 ± 0.02, $n = 4$) vs. 0.3 pH units for ROMK (7.2 ± 0.1 to 6.9 ± 0.03, $n = 4$). Consequently, elevation of external [K] in the range of normal internal pH (*thin rectangle*, Fig. 5) would produce a much smaller increment in whole-cell conductance for C9 than for ROMK.

Extracellular Cs was also effective in activating ROMK channels. The time course for activation (half time ~3 min) and deactivation (half time ~5 min) of ROMK was similar, but not strictly comparable, for both external Cs and 10 mM K (Fig. 6). Activation by external Cs is consistent with an effect of external Cs on ROMK pH sensitivity, similar to the action of K on ROMK pH sensitivity (Fig. 4). This was examined using the cut-open oocyte preparation (Fig. 7). At a constant 1 mM external K, addition of 104 mM Cs (replacing Na) shifted the apparent pH sensitivity of ROMK oocytes by 0.4 pH units in an acid direction from an apparent pK_a of 7.2 ± 0.1 ($n = 6$) in 1 mM K to an apparent pK_a of 6.8 ± 0.01 ($n = 4$) in cesium (Fig. 7). In the range of normal pH (*rectangle*, Fig. 7) Cs activation of ROMK was similar to K activation of ROMK, where the increase in whole-cell conductance could be thought of as a transition from the 1 K titration curve to the 104 Cs titration curve.

These results suggest that K and Cs both interact with the external side of ROMK to affect pH gating. Therefore, we examined whether a toxin known to specifically interact with the outside of the channel also affected pH gating. Recent studies with a toxin derived from honeybee venom have established that TPNQ specifically interacts with the external surface of ROMK but not IRK1, and that one molecule of TPNQ binds to one ROMK, with an inhibition constant (K_i) of 8.6 nM (Jin and Lu, 1998; Jin et al., 1999).

As shown in Fig. 8, 2 μM TPNQ reversibly inhibited ROMK whole-cell conductance in oocytes maintained in 10 mM external K and buffered with pH 7.8 acetate solutions. Outward conductances were normalized to the steady-state conductance before block. Half-maximal block and unblock occurred at 5 ± 1 min ($n = 7$), where ~1 min was required for a 95% solution exchange. Washout of TPNQ was associated with a small (17 ± 8%) but significant ($P < 0.05$, $n = 7$) overshoot of outward conductance (Fig. 8). This suggested that TPNQ was not only blocking ROMK but possibly stimulating ROMK as well.

Clearer evidence that TPNQ binding stimulated ROMK is illustrated in Fig. 9. ROMK oocytes were first inactivated by a 40–50 min preincubation in 1 mM K plus 55 mM acetate,

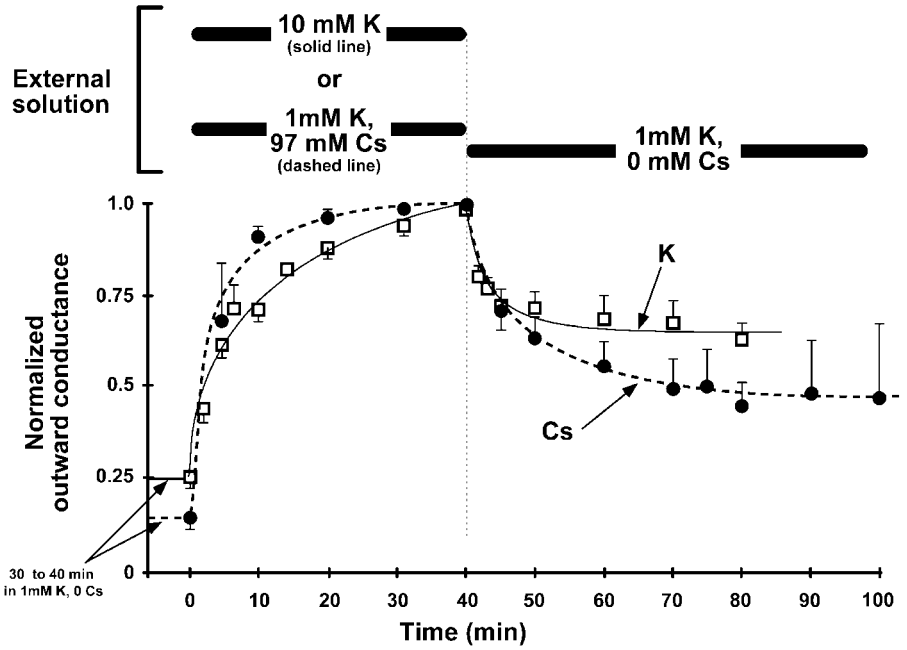

FIGURE 6 Similar activation and inactivation of ROMK by either external K or Cs. After incubation in 1 mM external K solutions, ROMK channels were activated by either 10 mM external K (*open squares, solid line*) or 97 mM external Cs (*solid circles, dashed line*). Return to 1 mM K, 0 Cs external solutions inactivated the conductance. In both cases, intracellular pH was maintained at 7.04, using a 7.8 permeant acetate buffer. Whole cell outward conductance was determined as the linear chord conductance (G) between the resting potential and 60-mV positive of the resting potential, using 25-ms voltage pulses at 20-mV increments. Between pulse cycles the membrane was unclamped. In each experiment, data were normalized to the maximum outward conductance. For the 10-mM K activation: avg. initial $G = 80 \pm 9$ μS, avg. Max $G = 343 \pm 36$ μS ($n = 31$), half time for activation $= 5.2 \pm 0.6$ min. For the Cs activation: avg. initial $G = 39 \pm 9$ μS, avg. Max $G = 285 \pm 46$ μS ($n = 6$), half time for activation $= 3.1 \pm 0.2$ min. Half times for deactivation were not significantly different.

buffered to a pH_o of 7.8. This corresponds to time 0 in Fig. 9. At this point, application of 2 μM TPNQ blocked ROMK outward conductance by more than 90% in 10 min. Washout of TPNQ (at constant 1 mM external K) not only reversed the block but also produced a large overshoot in outward conductance (*solid line*, *closed circles*, Fig. 9). Three min after washout of 2 μM TPNQ, outward conductance had doubled relative to pre-TPNQ values. Forty min after washout of TPNQ, outward conductance had increased by a factor of 3.7 ± 0.5 ($n = 14$) relative to its initial value.

Lower concentrations of TPNQ (0.02 μM) produced about the same stimulation of ROMK, (*dotted line*, *open squares*, Fig. 9). If TPNQ both blocks and stimulates ROMK, then washout of the lower TPNQ concentration would be expected to produce a faster unmasking of activation, consistent with the dotted line of Fig. 9.

A similar TPNQ protocol was applied to a chimera (C9) that is known to be insensitive to external K (Sackin et al., 2001) and to a point mutant of ROMK (K61M) that lacks pH

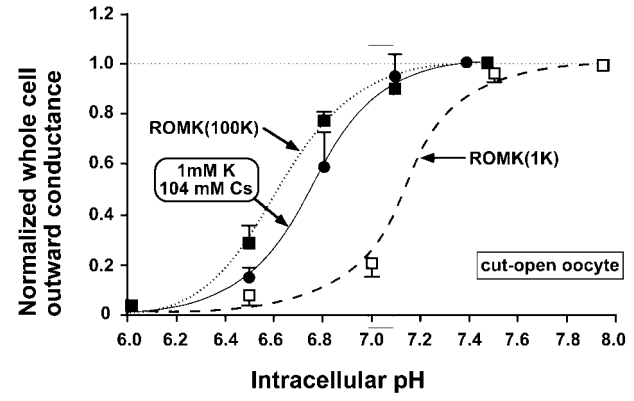

FIGURE 7 External K and Cs produce similar alteration in ROMK pH-dependence. The pH gating of ROMK2 was examined at different extracellular [K], using the perfused, cut-open oocyte technique (Methods). (*Open squares, dashed line*) ROMK2 in 1 mM external K (apparent $pK_a = 7.2 \pm 0.1$, $n = 6$). (*Solid squares, dotted line*) ROMK2 in 100 mM external K (apparent $pK_a = 6.6 \pm 0.03$ $n = 5$). (*Solid circles, solid line*) ROMK2 in 1 mM external K + 104 mM Cs (apparent $pK_a = 6.8 \pm 0.01$, $n = 4$). (*Thin rectangle*) Denotes approximate region of normal intracellular pH.

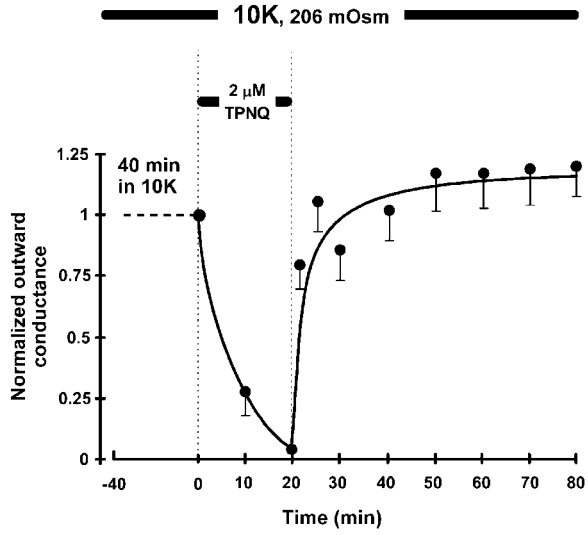

FIGURE 8 Reversibility of TPNQ block in 10 mM external K solutions. The intracellular pH of oocytes expressing ROMK was controlled with a permeant acetate buffer at $pH_o = 7.8$, corresponding to an internal oocyte pH_i of 7.04 (see Methods). Application of 2 μM TPNQ blocks 90% of the outward ROMK conductance. Washout of TPNQ in 10 mM external K produces a slight stimulation of outward conductance. In each experiment the data were normalized to the initial conductance in 10 mM K. The average initial ROMK conductance after 40 min in 10 mM K solution was 406 ± 66 μS ($n = 7$).

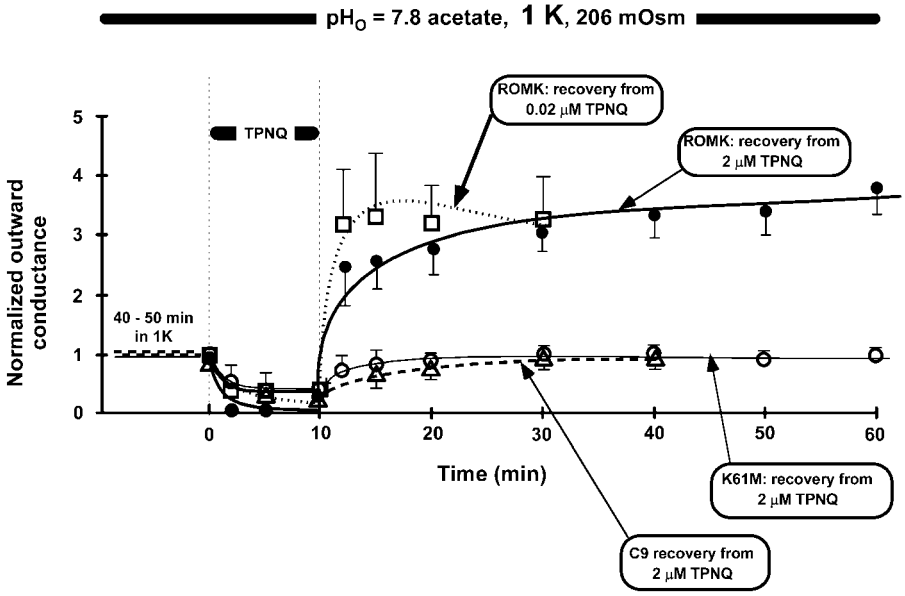

FIGURE 9 TPNQ stimulation of ROMK but not K61M or C9, in 1 mM external K. Data obtained from TEVC on ROMK oocytes in external acetate solutions (pH 7.8, 215 mOsm) to control intracellular pH. This corresponds to an intracellular pH of 7.04, using the calibration $pH_i = (0.595) \times pH_o + 2.4$ (see Methods). Oocytes unclamped in all intervals between conductance measurements. All conductances normalized to the initial conductances in 1 mM K with no TPNQ ($t = 0$), which were as follows: ROMK (*solid circles*), 119 ± 31 μS ($n = 18$); ROMK (*open squares*), 83 ± 18 μS ($n = 5$); K61M (*open circles*), 289 ± 22 μS ($n = 5$); and C9 (*open triangles*) 287 ± 20 μS ($n = 2$).

sensitivity (Sackin et al., 2001; Fakler et al., 1996). As indicated in Fig. 9, binding and washout of TPNQ from either C9 or K61M restored outward conductance to approximately its control value, but in neither case was there an overshoot or significant stimulation of whole-cell conductance during washout.

Inasmuch as external K activates ROMK by shifting the apparent pH sensitivity of the channel (Fig. 4), TPNQ might also activate ROMK by altering its pH sensitivity. The effect of 2 μM TPNQ on the apparent pH sensitivity of ROMK was examined (Fig. 10), using intact oocytes and permeant acetate buffers. The data in Fig. 10 were not normalized because intact oocytes in 1 mM external K cannot be alkalinized sufficiently to reach a maximal conductance. Nonetheless, 2 μM TPNQ produced a clear shift in the apparent pK_a. Hence, activation of ROMK channels by TPNQ at normal intracellular pH (*rectangle*, Fig. 10) can be thought of as a transition from the 1 K curve to the TPNQ curve in Fig. 10.

To assess whether TPNQ activation is a consequence of channel block per se or whether it depends on the specific interaction with ROMK, another blocker, δ-dendrotoxin, was applied to ROMK2 oocytes (Fig. 11). Delta-dendrotoxin is a neurotoxin isolated from the venom of the green mamba snake, that was shown to specifically block $K_{ir}1.1$ (ROMK) and $K_v1.1$ (Imredy et al., 1998). Mutational analysis indicated that δ-dendrotoxin binds strongly to the extracellular ''turret'' region of ROMK (corresponding to the MP region in Fig. 1) without completely blocking the channel (Imredy et al., 1998). This differs from the manner in which TPNQ interacts with ROMK (Jin et al., 1999).

In our studies, a 10-min exposure to 1 μM δ-dendrotoxin blocked 62 ± 9% (n = 5) of whole-cell ROMK conductance, which is significantly less than the 90 ± 4% ($n = 11$) block produced by similar concentrations of TPNQ. Even though δ-dendrotoxin was a less effective blocker than TPNQ, it was clearly interacting with the extracellular side of ROMK (Imredy et al., 1998). However, in contrast to TPNQ, binding and washout of δ-dendrotoxin produced no significant stimulation of ROMK whole-cell conductance (Fig. 11). Hence, the observed activation of ROMK by TPNQ depends on the specific interaction between this blocker and the extracellular surface of ROMK.

DISCUSSION

K modulation of pH gating

Fig. 2 confirms that external K both activates ROMK in a dose-dependent manner and modulates its pH sensitivity.

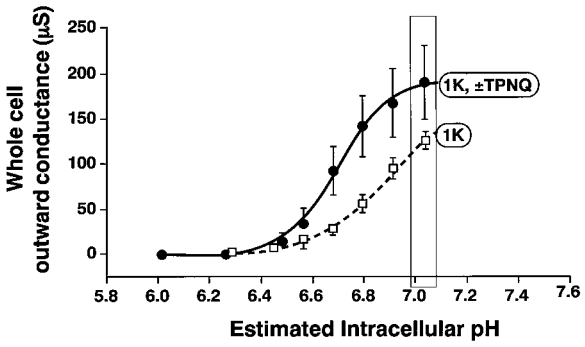

FIGURE 10 Application and washout of TPNQ shifts the pH sensitivity of ROMK. Two-electrode voltage clamp experiments, where intracellular pH was directly controlled by changing extracellular pH using a permeant acetate buffer. Intracellular pH was computed from extracellular pH using the linear calibration $pH_i = (0.595) \times pH_o + 2.4$ (see Methods). (*Open squares*) ROMK2 in 1 mM K (apparent $pK_a = 6.9 \pm 0.04$, estimated maximal conductance = 160 ± 20 μS, $n = 7$). (*Solid circles*) ROMK2 after exposure and washout of 2 μM TPNQ washout (apparent $pK_a = 6.7 \pm 0.04$, estimated maximal conductance = 190 ± 12 μS, $n = 7$). (*Thin rectangle*) Denotes approximate region of normal intracellular pH.

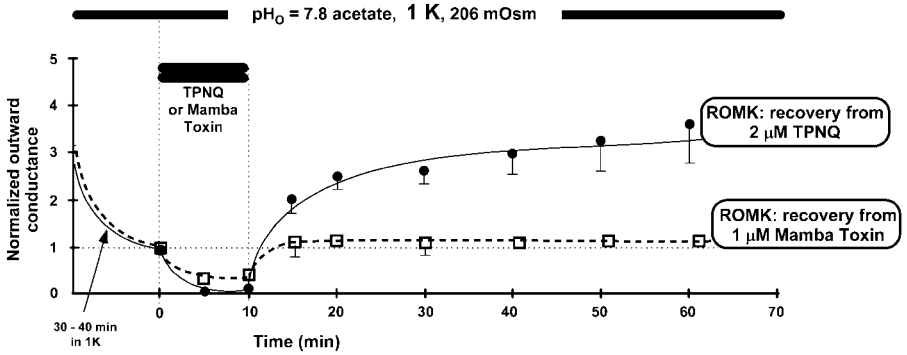

FIGURE 11 TPNQ, but not Mamba Toxin (δ-dendrotoxin), activates ROMK. Data obtained from paired TEVC experiments on intact ROMK oocytes in external acetate solutions (pH 7.8, 215 mOsm) to control intracellular pH. This corresponds to an intracellular pH of 7.04, using the calibration: $pH_i = (0.595) \times pH_o + 2.4$ (see Methods). Oocyte unclamped in all intervals between conductance measurements. All conductances normalized to the steady-state conductance in 1 mM K with no toxin: ROMK (*solid circles*) 143 ± 37 μS ($n = 11$); and ROMK (*open squares*) 189 ± 33 μS ($n = 5$).

When external K is 10 mM (or higher), acid deactivation of ROMK is rapidly reversible (Fig. 2, *D* and *E*); whereas in 1 mM external K, the same acid deactivation cannot be readily reversed by alkalization (Fig. 2, *A* and *B*).

This dependence of ROMK pH sensitivity on external K is illustrated more directly by the titration curves of Figs. 4, 5, and 7 which were obtained with cut-open oocytes in which internal pH was directly controlled by the oocyte perfusion. These results indicated that ROMK pH gating was strongly dependent on external K, where the apparent pK_a of the channel was shifted from 7.2 ± 0.1 in 1 mM K, to 6.9 ± 0.03 in 10 mM K, and then to 6.6 ± 0.03 in 100 mM K (Fig. 4). At any given internal pH, raising external K increased whole-cell conductance by activating more ROMK channels, consistent with a vertical transition from the 1-K, to the 10-K, to the 100-K titration curves (Fig. 4). This confirms previous reports on the interaction between external K and internal pH in ROMK channels (Sackin et al., 2001; Doi et al., 1996; Schulte et al., 2001).

It should be noted that the pH curves of Figs. 4, 5, and 7 were all obtained by progressively decreasing internal pH, using each oocyte as its own control. Hysteresis effects at low external K (Figs. 2 and 3) result in different pH titration curves depending on whether pH is decreased or increased in a given oocyte.

A three-state model for ROMK activation

The interaction between internal hydrogen ion and external K can be understood in terms of a three-state sequential model (Fig. 12) in which low K stabilizes the closed conformation of the channel. This model was first proposed for ROMK1 (K_{ir} 1.1a) by Schulte et al. (2001). In the present treatment, we compare this model to a second scheme in which high K stabilizes the open conformation of the channel (Fig. 14). Analysis of both models indicated that the first model (Fig. 12) better described the relationship between external K and the apparent K_i for internal protons (Fig. 13). Therefore, we adopted this model of one-active and two-inactivated states (Fig. 12) as a framework for understanding the experimental results. It incorporates the binding of multiple H^+ ions and contains a number of simplifying assumptions, which are enumerated at the beginning of the Appendix.

Essentially, the model hypothesizes one active, deprotonated state A(K,0) in which K is bound but hydrogen is not; and two inactivated protonated states, one of which has a bound K, I(K,H), and another which lacks K, I(0,H). The model is sequential, with forward and backward rate constants k_1, k_2, k_3, and k_4. Transitions between I(0,H) and A(K,0) must proceed through the intermediate inactive state: I(K,H). Inasmuch as ROMK2 has four subunits, up to $\alpha =$ four protons might be required to move from the active A(K,0) state to the inactivated I(K,H) state. Mutation of the putative pH sensor (ROMK2-K61M) renders the channel insensitive to internal pH above 6.5, suggesting that this mutation blocks A(K,0) to I(K,H) transition and these channels will always be in the active state. Other mutations (indicated by C9, F129C, L117I, and V121T in Fig. 12)

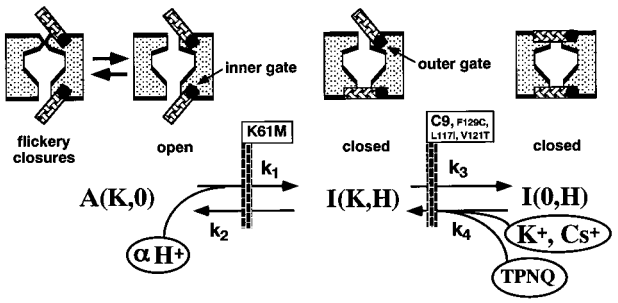

FIGURE 12 Two-gate model for the interaction between external K and internal pH. The two-gate model consists of two structurally independent but functionally interactive gates: (*1*) an outer K-sensitive gate, consisting of the selectivity filter itself, and (*2*) an inner pH-sensitive gate. There is a direct correspondence between the two-gate model and a three-state sequential kinetic model shown underneath. In the kinetic model, the active state A(K,0) requires both the binding of external K and deprotonation of the putative pH gate at K61. The inactivated I(K,H) state is reached by protonation of the active state by as many as α-protons. This pathway is blocked by the mutation ROMK2-K61M which presumably prevents protonation of this site. The inactivated I(0,H) state is reached by removal of external K. This pathway is blocked by several mutations in the PM region (C9 chimera, F129C) as well as two mutations in the pore region (V121T and L117I). Elevation of external K, addition of Cs, or application of the specific blocker TPNQ, all enhance deprotonation by shifting the equilibrium from I(0,H) to I(K,H).

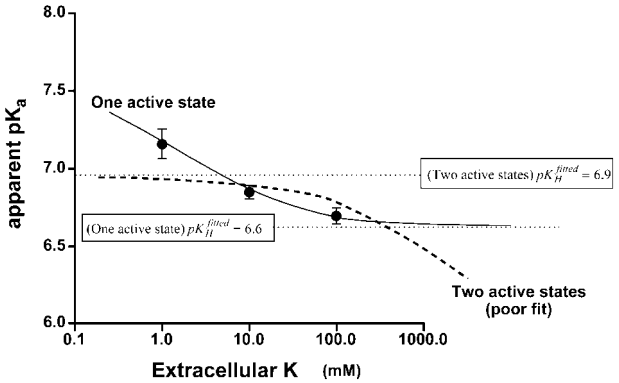

FIGURE 13 Fit of the pH titration data to the three-state model. The complete set of pH titration data obtained with cut-open, perfused oocytes data were fit to two alternative three-state models (Figs. 12 and 14). Both models predicted that ~3 protons would bind to the active state ($\alpha = 3$). The best fit for the one-active (two-inactive) model gave a fitted pK_H of 6.6, which corresponds to the limiting value of apparent pK_a at high external [K]. The best fit for the two-active (one-inactive) model gave a fitted pK_H of 6.9, which corresponds to the limiting value of apparent pK_a at small external [K]. As can be seen, the one-active-state model (*solid line*) fits the data better than the two-active-state model (*dashed line*).

render the channel insensitive to external K by blocking the transition from I(K,H) to I(0,H).

Predictions of the three-state model

The equilibrium equations for the three-state model of Fig. 12 are summarized in the Appendix. The cut-open data of Fig. 4 were used to fit this model, assuming the following three free parameters:

1. α = number of H^+ required to inactivate the channel;
2. K_H = the equilibrium constant for the proton binding step
3. K_K = the equilibrium constant for the K binding step.

Employing a variety of different weighting schemes, the least-squares best fit to the complete cut-open data set were as follows:

1. $3.2 > \alpha > 2.9$
2. $K_H = 10^{-6.6}$ M
3. $K_K = 48$ mM

Values of α between 2.7 and 3.2 are consistent with the requirement that transitions between the active state A(K,0) and the first inactivated state I(K,H) require the binding of three protons. An important prediction of the model in Fig. 12 is that the relationship between apparent pK_a and extracellular Log[K] will be concave upward, with the apparent pK_a approaching pK_H ($= -\mathrm{Log}_{10} K_H = 6.6$) at high K concentration (Fig. 13).

We also derived steady-state equations for an alternative three-state model consisting of two active states and one inactivated state, in which $[K]_{ext}$ stabilizes the open state. This model also accounts for the K-dependence of the apparent pK_a values. However, this alternative model predicts a concave downward relationship between apparent pK_a and extracellular Log[K] (*dashed curve*, Fig. 13). This type of relation does not fit the apparent pK_a data of Fig. 4 as well as the model with one active state and two inactive states (Fig. 13), and no further evaluation of this model was conducted. The remainder of the Discussion focuses on the three-state model of Fig. 12.

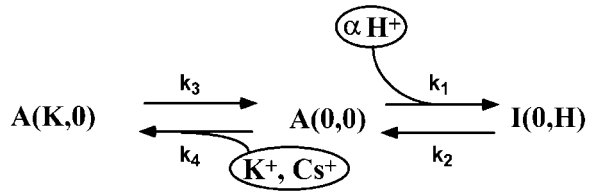

FIGURE 14 Alternate gating model: two open states, one closed state. This three-state model is an alternative to the model depicted in Fig 12. There are two active states, A(K,0) and A(0,0) and one inactivated state, I(0,H). The active state A(K,0) is stabilized by either external K or external Cs, and the inactivated state is reached by protonation of A(0,0) by as many as α-protons. The equations for this model are described in the Appendix. Fig. 13 compares the predictions of this model with those of the one-active-state model of Fig 12.

Although the equilibrium values of α, K_H, and K_K for the three-state model were first determined from the cut-open pH titrations as described above, it is also possible to obtain independent estimates for these three parameters from ROMK activation data at different external [K] (Fig. 2 *C*), provided one assumes that the conductance reaches a steady state after a 40-min exposure to high K. Although this assumption is not rigorously correct, it turns out that the estimates of alpha and pK_H obtained from these experiments were quite similar to the estimates obtained with the cut-open pH data of Fig. 4 ($3.2 > \alpha > 2.9$; and $pK_H = 6.6$). However, the parameter fits to the K activation data of Fig. 2 *C* were insensitive to the values for the K equilibrium constant (40 mM $< K_K <$ 300 mM). Over this range of K_K, neither the goodness of fit nor the estimates of pK_H or alpha were strongly affected. Therefore, we have more confidence in values of K_K determined from fits to the pH titration data of Fig. 4, which yielded a best-fit of $K_K = 48$ mM.

The model provides a qualitative explanation for the hysteresis effects of Fig. 3. The extremely slow activation of ROMK in Fig. 3 *B* is a direct consequence of starting from the I(0,H) inactive state, assuming that the rate of leaving this state (for the I(K,H) state) is slow and rate-limiting. In contrast, in Fig. 3 *D*, the channels start from the active A(K,0) state so that the time course reflects the relatively rapid kinetics governing transitions between the A(K,0) and I(K,H) states. Although in principle it is possible to model the kinetic behavior more quantitatively by assigning individual rate constants for transitions between the three states, we were reluctant to do this inasmuch as alteration of internal pH required 10–15 min, with either permeant buffers or internal oocyte perfusion. Therefore, the time course of the conductance change reflects both the rate constants for

activation and inactivation as well as the rate constants for changing internal pH.

A structural basis for the three-state model

The kinetic model can be interpreted as two structurally independent, but functionally interactive, gates in series across the membrane: (*1*) an outer K-sensitive gate, consisting of the selectivity filter itself, and (*2*) an inner pH-sensitive gate, possibly formed by a section of the inner transmembrane helix that is hinged at a conserved glycine (Jiang et al., 2002a,b). This correspondence between kinetic and structural models is depicted in Fig. 12. It is based largely on high-resolution structural studies of KcsA in which the selectivity filter of the channel can assume either a ''high-K'' or a ''low-K'' configuration based on access of internal and external K to the selectivity site (Zhou et al., 2001).

Our experiments confirm that there is communication between the putative inner and outer gates of ROMK ($K_{ir}1.1$). However, the details of that communication are not yet resolved. One possibility is that K itself transduces information between the inner and outer gates of the channel. In this model, the interaction between external K and internal pH occurs because the outer (selectivity filter) gate is controlled by (*1*) availability of external K (or Cs or TPNQ), and (*2*) accessibility to high internal K, which is itself controlled by the inner pH gate. Closure of the pH gate deprives the selectivity filter gate of access to high internal K. If, at the same time, external K is also removed, the selectivity filter (outer) gate would switch from a high-K to a low-K configuration (Jiang et al., 2002b), placing the channel in its inactivated state: I(0,H) in Fig. 12.

Alternatively, inner gate closure may alter the conformation of the channel around the selectivity filter, causing the outer gate to inactivate when the bath contains zero K (Schulte et al., 2001). In support of this model, Schulte et al. showed that in excised patches, even complete removal of K from both sides of the membrane did not inactivate the channels when the internal pH was maintained at pH 8. This suggests that closing the pH gate does more than simply restrict access of K to the selectivity filter.

In this regard, communication between inner and outer gates may be different in KcsA and ROMK. In the former, K activity within the pore may be the signal for closure of the selectivity filter gate (in the absence of external K); whereas in ROMK, the inner (pH) gate and the outer (selectivity filter) gate probably communicate via subtle changes in protein conformation. Previous studies with ROMK have indicated that mutation of any of the five ROMK2 residues, F129, Q133, E132, V121, and L117, disrupts communication between the inner and outer gates and prevents the channel from entering the inactivated, I(0,H), state when K is removed from the bath (Sackin et al., 2001; Schulte et al., 2001). These ROMK mutants are still gated by internal pH, but not by external K.

The effect of TPNQ on ROMK conductance

The honeybee toxin derivative, TPNQ, reversibly blocked ROMK2 channels expressed in oocytes, consistent with previous results (Jin and Lu, 1998; Jin et al., 1999). However, the binding and washout of TPNQ also appeared to activate ROMK, which was somewhat unexpected. This effect of TPNQ is not an automatic consequence of unblocking the channel inasmuch as the binding and washout of δ-dendrotoxin produced no significant stimulation of ROMK whole-cell conductance (Fig. 11). Hence, activation of ROMK by TPNQ depends on a specific interaction between TPNQ and the outside surface of ROMK.

Several observations suggest that the interaction of the toxin with ROMK mimics that of extracellular K. First of all, neither external K nor TPNQ activated the K61M mutant of ROMK2 (Fig. 9). It is known that K61M mutants of ROMK2 remain in the activated state as long as internal pH is greater than 6.0 (Doi et al., 1996; Choe et al., 1997). Hence, neither external K nor TPNQ activated K61M because this mutant was already maximally activated.

More precise information about the effect of TPNQ binding comes from its effect on the C9 chimera (Fig. 9). Inasmuch as the C9 chimera disrupts the K-dependent transition between states I(0,H) and I(K,H) in Fig. 12, the inability of both K and TPNQ to activate C9 suggests that both external K and TPNQ are acting at the outer gate in the model of Fig. 12.

A second argument for TPNQ's mimicking the effect of external K comes from the finding that both K and TPNQ have a similar effect on the pH sensitivity of ROMK whole-cell conductance. Using a two-electrode voltage clamp with intact ROMK oocytes, 2μM TPNQ binding and washout shifted the apparent pK_a in an acid direction relative to the 1 mM K titration of the conductance titration curve from 6.9 to 6.7 (Fig. 10). This was qualitatively similar to what was observed with cut-open oocytes (Fig. 4). The shift in pK_a with TPNQ cannot be explained by a pH-dependent binding of TPNQ (Ramu et al., 2001) since the TPNQ conductances in Fig. 10 were determined 30 min after washout of the toxin.

To eliminate the possibility that TPNQ was interacting with a second high-affinity ''stimulatory'' site, we tested the effect of 20 picomolar TPNQ. This concentration neither blocked nor stimulated ROMK, and serves as a negative control, suggesting that ROMK activation by TPNQ only occurs if the channels are first blocked by TPNQ.

Prior studies have indicated that mutating the *Phe* residue at ROMK2 position 129 (F148 in ROMK1) has a large effect on TPNQ binding (Jin et al., 1999). This is precisely the residue that also has the largest effect on activation of ROMK by external K or Cs (see Fig. 13 in Sackin et al., 2001). In contrast, δ-dendrotoxin interacts (Imredy et al., 1999) most strongly with a *Glu* at ROMK2 position 104 (E123 in ROMK1). Residues in this region of ROMK did not seem to be crucial in mediating a response to external K

(Sackin et al., 2001), consistent with a lack of ROMK stimulation after δ-dendrotoxin (Fig. 11). Hence, the effect of TPNQ on ROMK may involve a specific interaction between the toxin and one or more extracellular sites on ROMK.

Inasmuch as TPNQ increased the number of ROMK active channels, TPNQ must be binding to a significant number of inactivated channels and destabilizing the low-K (collapsed) configuration of the selectivity filter. Washout of TPNQ would then unmask a now-open selectivity filter gate. Hence, TPNQ binding may activate ROMK conductance by preventing collapse of the outer gate of the channel in much the same way that the ROMK2 mutations, F129, E132, and Q133 in the extracellular region, prevent collapse by stabilizing the high-K configuration of the selectivity filter.

The sustained effects of TPNQ on ROMK channel activation shown in Figs. 9 and 11 are puzzling. Detailed information about the interaction surfaces of TPNQ and ROMK (Jin et al., 1999) suggests that the α-helical region of TPNQ fits into the outer mouth of the channel pore. If TPNQ produced a similar but more stable conformational change in ROMK than either K or Cs, the TPNQ effect might persist long after the toxin is removed.

APPENDIX

The three-state model of Fig. 12: one open state, two closed states; a three-parameter fit using the complete data set

The following assumptions are inherent in the three-state, sequential model of Fig. 12.

1. There is one active, deprotonated state A(K,0) in which K is bound but hydrogen is not; and two inactivated protonated states, one of which has a bound K, I(K,H), and the other does not, I(0,H). K conduction in A(K,0) may be transiently interrupted by flickery closures.
2. Protonation of a fixed number alpha (α) of sites on the interior of the channel gates the channel closed.
3. External potassium (K) binds only to the inactive, protonated state I(0,H).
4. The open state A(K,0) requires both the presence of external K (or Cs) and the deprotonation of an internal pH sensor (K61 in ROMK2 or K80 in ROMK1).
5. Multiple protons bind to the A(K,0) state independent of each other.

Let K_H and K_K be the equilibrium constants, respectively, for the left and right sides of the reaction in Fig. 12, where

$$(K_H)^{\alpha} = \frac{k_2}{k_1} \tag{A1}$$

$$K_K = \frac{k_3}{k_4} \tag{A2}$$

In the steady state:

$$A(K,0)[H]^{\alpha} \times k_1 = k_2 \times I(K,H) \tag{A3}$$

$$I(0,H)[K] \times k_4 = k_3 \times I(K,H) \tag{A4}$$

Eliminating the middle state I(K,H) from these two equations, and solving for I(0,H):

$$I(0,H) = A(K,0)\left(\frac{[H]}{K_H}\right)^{\alpha} \times \frac{K_K}{[K]} \tag{A5}$$

Equation A.4 also allows expression of I(K,H) in terms of A(K,0):

$$I(K,H) = A(K,0)\left(\frac{[H]}{K_H}\right)^{\alpha} \tag{A6}$$

Let N = total number of channels in all three states:

$$N = A(K,0) + I(K,H) + I(0,H) \tag{A7}$$

Substituting I(K,H) and I(0,H) from Eq. A.6 and Eq. A.5 into Eq. A.7, and solving for the number of channels in the open state A(K,0):

$$A(K,0) = \frac{N}{1 + \left(\frac{[H]}{[K_H]}\right)^{\alpha} \times \left(1 + \frac{K_K}{[K]}\right)} \tag{A8}$$

Hence, the predicted normalized conductance for this model is given by the ratio (F) of the number of active channels, A(K,0), to the total number of channels (N):

$$F = \frac{1}{1 + \left(1 + \frac{K_K}{[K]}\right) \times \left(\frac{[H]}{K_H}\right)^{\alpha}} \tag{A9}$$

The three model parameters: α, K_H, and K_K can be fit to the data on normalized whole-cell conductance as a function of the two independent variables [H] and [K], according to:

$$F = 1/(1 + (1 + K_K/[K]) \times (([H]/(10\hat{}(-pK_H^{fitted})))\hat{}\alpha)) \tag{A10}$$

Equation A.10 was solved using the solver function of Excel with the complete data set of normalized conductance at different internal pH and different external [K].

The fitted parameters of interest are:

1. α = number of H^+ interacting with the active state.
2. $pK_H^{fitted} = -Log_{10}K_H$.
3. K_K = equilibrium constant for the K binding step.

The apparent pK_a values, $pK_a^{app}(K)$, for each of the pH titration curves at different external [K], are related to the fitted value $pK_H^{fitted}(K)$ according to:

$$pK_a^{app}(K) = pK_H^{fitted} + \frac{1}{\alpha} Log_{10}\left(1 + \frac{K_K}{[K]}\right) \tag{A11}$$

From the form of Eq A.11, pK_H^{fitted} can be thought of as the limiting value of pK_a^{app} (K)at large external [K]:

$$pK_H^{fitted} = \lim_{[K]\to\infty} pK_a^{app}(K) \tag{A12}$$

Equations A.12 and A.13 were used to draw the smooth curves in Fig. 13 for the model with one active state and two inactive states (Fig 12).

An alternative model: two open states and one closed state (Fig. 14)

An alternative to the model of Fig 12, in which external K stabilizes the open state, is shown in Fig. 14. In this model, there are two active states: A(K,0) and A(0,0). Protonation drives channels from A(0,0) into an inactive state I(0,H). The equations are analogous to those developed for the one-open, two-closed state. The equilibrium constants for K and protons are defined according to Eqs. A1 and A2, but Eqs. A5 and A6 are replaced by:

$$I(0,H) = A(0,0)\left(\frac{[H]}{K_H}\right)^{\alpha} \quad \text{(A13)}$$

$$A(0,0) = A(K,0)\left(\frac{K_K}{[K]}\right) \quad \text{(A14)}$$

If N is the total number of channels in all three states, then

$$N = A(K,0) + A(0,0) + I(0,H) \quad \text{(A15)}$$

and the total number of active channels (= ACTIVE) is given by:

$$ACTIVE = A(K,0) + A(0,0) = A(K,0)\left[1 + \frac{K_K}{[K]}\right] \quad \text{(A16)}$$

Combining Eqs. A.13–A.15:

$$A(K,0) = \frac{N}{1 + \left(\frac{K_K}{[K]}\right) + \left(\frac{K_K}{[K]}\right) \times \left(\frac{[H]}{K_H}\right)^{\alpha}} \quad \text{(A17)}$$

Inasmuch as ROMK whole-cell current in these experiments is directly related to the number of ACTIVE channels, the predicted normalized conductance for this model is given by the ratio (F) of the number of ACTIVE channels to the total number of channels (N),

$$F = \frac{1}{1 + \left(\frac{K_K}{[K] + K_K}\right) \times \left(\frac{[H]}{K_H}\right)^{\alpha}} \quad \text{(A18)}$$

or in Excel notation:

$$F = 1/(1 + (K_K/([K] + K_K)) \times (([H]/(10\text{^}(-pK_H^{fitted})))\text{^}\alpha)) \quad \text{(A19)}$$

The apparent pK_a values, $pK_a^{app}(K)$, for each of the pH titration curves at different external $[K]$ are related to the fitted value of pK_H^{fitted} according to:

$$pK_a^{app}(K) = pK_H^{fitted}(K) - \frac{1}{\alpha}\mathrm{Log}_{10}\left(1 + \frac{[K]}{K_K}\right) \quad \text{(A20)}$$

From the form of Eq. A.20, pK_H^{fitted} can be thought of as the limiting value of $pK_a^{app}(K)$at small external $[K]$:

$$pK_H^{fitted} = \lim_{[K]\to 0} pK_a^{app}(K) \quad \text{(A21)}$$

Equations A.20 and A.21 were used to draw the smooth curves in Fig 13 for the model with two active states and one inactive state.

Although Eq. A.20 is similar to Eq. A.11, there are some important differences that distinguish the two models. Eq. A.11 predicts a functional relationship between $pK_a^{app}(K)$ and external Log[K] that is concave upward, whereas Eq. A.20 predicts a concave downward relation between $pK_a^{app}(K)$ and external Log[K]. Hence, the two models can be distinguished by Fig 13.

This work was supported by National Institutes of Health grants DK46950 (H.S.) and DK27847 (LG.P.).

REFERENCES

Choe, H., L. G. Palmer, and H. Sackin. 1999. Structural determinants of gating in inward-rectifier K^+ channels. *Biophys. J.* 76:1988–2003.

Choe, H., H. Zhou, L. G. Palmer, and H. Sackin. 1997. A conserved cytoplasmic region of ROMK modulates pH sensitivity, conductance, and gating. *Am. J. Physiol.* 273:F516–F529.

Costa, A., J. Patrick, and J. Dani. 1994. Improved technique for studying ion channels expressed in Xenopus oocytes, including fast superfusion. *Biophys. J.* 67:395–401.

Doi, T., B. Fakler, J. H. Schultz, U. Schulte, U. Brandle, S. Weidemann, H. P. Zenner, F. Lang, and J. P. Ruppersberg. 1996. Extracellular K^+ and intracellular pH allosterically regulate renal Kir1.1 channels. *J. Biol. Chem.* 271:17261–17266.

Fakler, B., J. H. Schultz, J. Yang, U. Schulte, U. Brandle, H. P. Zenner, L. Y. Jan, and J. P. Ruppersberg. 1996. Identification of a titratable lysine residue that determines sensitivity of kidney potassium channels (ROMK) to intracellular pH. *EMBO J.* 15:4093–4099.

Horton, R. M., H. D. Hunt, S. N. Ho, J. K. Pullen, and L. R. Pease. 1989. Engineering hybrid genes without the use of restriction enzymes: gene splicing by overlap extension. *Gene.* 77:61–68.

Imredy, J., C. Chen, and R. MacKinnon. 1998. A snake toxin inhibitor of inward rectifier potassium channel ROMK1. *Biochemistry.* 37:14867–14874.

Jiang, Y., A. Lee, J. Chen, M. Cadene, B. Chalt, and R. MacKinnon. 2002a. Crystal structure and mechanism of a calcium-gated potassium channel. *Nature.* 417:515–522.

Jiang, Y., A. Lee, J. Chen, M. Cadene, B. Chalt, and R. MacKinnon. 2002b. The open pore conformation of potassium channels. *Nature.* 417:523–526.

Jin, W., A. Klem, J. Lewis, and Z. Lu. 1999. Mechanisms of inward-rectifier K channel inhibition by Tertiapin-Q. *Biochemistry.* 38:14294–14301.

Jin, W., and Z. Lu. 1998. A novel high-affinity inhibitor for inward-rectifier K channels. *Biochemistry.* 37:13291–13299.

Leipziger, J., G. MacGregor, G. Cooper, J. Xu, S. Hebert, and G. Giebisch. 2000. pK_a site mutations of ROMK2 channels shift the pH dependence to more alkaline values. *Am. J. Physiol.* 279:F919–F926.

McNicholas, C. M., G. G. MacGregor, L. D. Islas, Y. Yang, S. C. Hebert, and G. Giebisch. 1998. pH-dependent modulation of the cloned renal K^+ channel, ROMK. *Am. J. Physiol.* 275:F972–F981.

McNicholas, C. M., W. Wang, K. Ho, S. C. Hebert, and G. Giebisch. 1994. Regulation of ROMK1 K^+ channel activity involves phosphorylation processes. *Proc. Natl. Acad. Sci. USA.* 91:8077–8081.

Palmer, L. G., H. Choe, and G. Frindt. 1997. Is the secretory K channel in the rat CCT ROMK? *Am. J. Physiol.* 273:F404–F410.

Perozo, E., D. M. Papazian, E. Stefani, and F. Bezanilla. 1992. Gating currents in Shaker K^+ channels. Implications for activation and inactivation models. *Biophys. J.* 62:160–171.

Ramu, Y., A. Klem, and Z. Lu. 2001. Titration of Tertiapin-Q inhibition of ROMK1 channels by extracellular protons. *Biochemistry.* 40:3601–3605.

Sackin, H., S. Syn, L. G. Palmer, H. Choe, and E. Walters. 2001. Regulation of ROMK by extracellular cations. *Biophys. J.* 80:683–697.

Schulte, U., S. Weidemann, J. Ludwig, J. Ruppersberg, and B. Fakler. 2001. K-dependent gating of Kir1.1 channels is linked to pH gating through a conformational change in the pore. *J. Physiol.* 534: 49–58.

Taglialatela, M., L. Toro, and E. Stefani. 1992. Novel voltage clamp to record small fast currents from ion channels expressed in Xenopus oocytes. *Biophys. J.* 61:78–82.

Tsai, T. D., M. E. Shuck, D. P. Thompson, M. J. Bienkowski, and K. S. Lee. 1995. Intracellular H^+ inhibits a cloned rat kidney outer medulla K^+ channel expressed in *Xenopus* oocytes. *Am. J. Physiol.* 268: C1173–C1178.

Wang, W., H. Sackin, and G. Giebisch. 1992. Renal potassium channels and their regulation. *Annu. Rev. Physiol.* 54:81–96.

Wang, W. H., and G. Giebisch. 1991. Dual modulation of renal ATP-sensitive K^+ channel by protein kinases A and C. *Proc. Natl. Acad. Sci. USA.* 88:9722–9725.

Zhou, Y., J. Morais-Cabral, A. Kaufman, and R. MacKinnon. 2001. Chemistry of ion coordination and hydration revealed by a K channel Fab complex at 2.0Å resolution. *Nature.* 414:43–48.